Extended Photon Counting Histogram and Fluorescence Intensity Distribution Analysis Approaches for Optically Biased Photon Counting Statistics

Fanbo Meng[†] and Hui Ma*[,†,‡]

Graduate School at Shenzhen, Tsinghua University, Shenzhen 518055, China, and Department of Physics and The Key Lab of Atomic and Molecular Nano Sciences, Ministry of Education, Tsinghua University, Beijing 100084, China

Received: December 5, 2005; In Final Form: March 12, 2006

A gradient potential induced by a strongly focused laser beam can perturb the diffusion dynamics of particles in solutions and result in biased photon counting statistics in fluorescence fluctuation spectroscopy (FFS). In this paper, the theories of the photon counting histogram (PCH) and fluorescence intensity distribution analysis (FIDA) approaches are extended independently to fit the biased experimental data and retrieve the unbiased parameters, i.e., the average number of the sample particles in the focal volume N, their brightness ϵ, and polarizability α. The extended theories are tested using Monte Carlo simulations for single- and double-component systems. It is also proved numerically and analytically that the extended PCH and FIDA approaches are completely equivalent. Practical implementations and possible applications of extended PCH and FIDA are discussed.

1. Introduction

Fluorescence fluctuation spectroscopy (FFS)[1] is a suite of ultrasensitive detection techniques based on temporal fluorescence signal analysis. The most prominent examples of FFS include fluorescence correlation spectroscopy (FCS)[2−6] and photon counting histogram (PCH)[7,8] or its equivalent, fluorescence intensity distribution analysis (FIDA).[9] The former analyzes the correlation function of the fluorescence photon counts and retrieves the average number N of the fluorophores in the laser focal volume and their average diffusion time τ_D through the focal volume. The latter analyzes the histogram, i.e., the probability $P(k)$ of detecting k fluorescence photons in a sampling time, and retrieves N and the brightness ϵ of the fluorophores. Since its first appearance in the 1970s, FFS has been finding more and more applications in different biological and chemical systems.

Intense excitation lasers and high numerical aperture (NA) objectives are often adopted in FFS experiments to improve the signal-to-noise ratio (SNR) or facilitate multiphoton excitation. In such cases, the tightly focused intense laser beam can generate a gradient force, known as the "optical trap" or "optical tweezers", on the particles being monitored in the sample solution.[10−13] The gradient field may become strong enough to alter the diffusion dynamics of the particles and manifest itself in biased photon statistics.[14,15] If not handled properly, the laser gradient field can interfere with the FCS and PCH (FIDA) experiments and result in systematic errors in the retrieved parameters.

Studies on FFS techniques in a gradient field have more profound significance. Optical trapping has become very popular in many biological and medical applications for biomanipulation and biosensing.[16,17] It has been used to probe the viscoelastic properties of DNA or cell membranes,[18] to evaluate the force exerted by molecular motors,[19] and to boost cluster formation.[20] The combination of the microscopic manipulation by optical trapping and the sensitive microscopic detection by FFS may offer a powerful tool for probing dynamic processes in living cells.

Effects of a gradient field on FCS detections have been studied numerically and analytically.[15,21−24] However, studies on biased PCH or FIDA remain relatively elementary. Early studies on biased photon counting distribution concentrate on the photon burst interval distribution,[14,15] which is not widely used due to its qualitative nature. Chirico studied qualitatively the effect of a harmonic trapping force on the photon statistics using Monte Carlo simulations and theoretical calculations.[25] However, a harmonic force approximation only applies when the potential is much stronger than the thermal energy and the particles are near the center of the focal spot.

In this paper, both PCH and FIDA are extended to analyze quantitatively the photon counting spectra in a laser gradient field. The extended models fit the biased photon counting statistics and retrieve the unbiased parameters, i.e., the average number N of the sample particles in the focal volume, their brightness ϵ, and polarizability α, in single- and double-component systems. It is proved that both PCH and FIDA are equivalent.

2. Theory

2.1. Gradient Potential. A gradient potential is described by[10]

$$U(\vec{r}) = -\frac{\alpha}{2}\langle E^2(\vec{r})\rangle = -\frac{\alpha I_0}{2\epsilon_0 c n_m} W(\vec{r}) \qquad (1)$$

where α, $E(\vec{r})$, I_0, n_m, c, and ϵ_0 represent the polarizability of the particles, the electrical field strength of the laser field, the intensity at the center of the focused laser beam, the refractive index of the medium, the speed of light, and the dielectric

* Corresponding author. E-mail: mahui@tsinghua.edu.cn.
[†] Department of Physics and The Key Lab of Atomic and Molecular Nano Sciences.
[‡] Graduate School at Shenzhen.

10.1021/jp057055d CCC: $33.50
Published on Web 04/21/2006

constant of a vacuum. $W(\vec{r})$ is the normalized intensity profile of the focused laser beam, which satisfies $W(0) = 1$. For simplicity, the point-spread function (PSF) is chosen to be the same as $W(\vec{r})$. More generalized choices will be discussed later. The gradient force can be calculated by $\vec{F}(\vec{r}) = -\nabla U(\vec{r})$.

We defined a dimensionless "gradient coefficient" θ as the ratio of the potential depth of the laser gradient field to the thermal energy:

$$\theta = |\frac{U(0)}{k_B T}| = \frac{\alpha I_0}{2\epsilon_0 c n_m k_B T} \tag{2}$$

where k_B and T are the Boltzmann's constant and the Kelvin temperature. The coefficient θ is an important factor in our theory describing the effect of a laser gradient field.

2.2. Biased Diffusion Dynamics. There are two problems concerning the theoretical treatment of the optically biased photon counting spectra: the equilibrium concentration distribution and the number distribution of sample particles in any spatial volume. We will derive the extended theories based on the analysis of these two problems.

In the presence of a gradient potential, the equilibrium concentration is no longer a constant but a distribution determined by the Boltzmann distribution or the Smoluchowski equation:[23,26]

$$C(\vec{r}) = C_0 e^{-U(\vec{r})/k_B T} = C_0 e^{\theta W(\vec{r})} \tag{3}$$

where C_0 is the unbiased concentration without a gradient potential or, equivalently, the concentration far from the focal spot. Since a gradient potential only affects an extremely small part of the solution, the increase in the concentration around the focal spot due to the gradient potential does not lead to a decrease in C_0.

It is known that the particle number in any spatial volume follows a Poisson distribution at a constant concentration. We will show that the Poisson distribution still applies in the presence of a potential. The average particle number n in any given volume V is a constant (does not change with time) for a given concentration distribution $C(\vec{r})$. First, we consider the problem in a larger volume V_L which encloses V. If the total particle number in V_L is n_L, each particle has a chance n/n_L to be in V. So, the particle distribution in V follows a binomial distribution:

$$P(k, n, n_L) = C_{n_L}^k \left(\frac{n}{n_L}\right)^k \left(1 - \frac{n}{n_L}\right)^{n_L - k} \tag{4}$$

When we expand V_L (thus n_L) to be infinitely large, the binomial distribution approaches a Poisson distribution with the average value n:

$$\mathrm{Poi}(k, n) = \frac{n^k e^{-n}}{k!} \tag{5}$$

The above analysis is based on a concentration distribution $C(\vec{r})$ but not a constant concentration, so the result still applies with the presence of a potential, provided that the concentration is in equilibrium.

2.3. Extended FIDA. The main idea of FIDA is that[9] the overall photon count spectrum is the convolution of photon count spectra from all the spatial volume elements dV_i, and the spectrum from any dV_i is determined by the number distribution of sample molecules and the shot noise, both of which can be described by a Poisson distribution:

$$P_i(k) = \sum_{n=0}^{\infty} \mathrm{Poi}(n, C_0\, dV_i)\, \mathrm{Poi}(k, n\epsilon W_i) \tag{6}$$

where ϵ is the brightness of the fluorescent particles. The first term in the multiplication represents the particle number distribution, and the second term represents the shot noise.

To avoid the convolution calculation, $P(k)$ is expressed in the generating function $G(\xi) = \sum P(k)\xi^k$. The term ξ is selected as $e^{i\phi}$, so $G(\xi)$ and $P(k)$ are connected by the Fourier transformation. Then, according to the convolution theorem, $G(\xi)$ is the product of all $G_i(\xi)$. This leads to[9]

$$G(\xi) = \exp(\int C_0\{\exp[(\xi - 1)\epsilon W(\vec{r})] - 1\}\, d\vec{r}) \tag{7}$$

On the basis of the discussion in section 2.2, we conclude that, in the presence of a laser gradient potential, the number distribution in dV_i follows a Poisson distribution of mean value $C(\vec{r}_i)\, dV_i$, where $\vec{r}_i$ is an arbitrary point in dV_i. So, eqs 6 and 7 still hold true if we replace C_0 by $C(\vec{r})$.

Using eq 3, one obtains

$$G(\xi) = \exp(\int C_0\{\exp[(\xi - 1)\epsilon W(\vec{r})] - 1\} e^{\theta W(\vec{r})}\, d\vec{r}) \tag{8}$$

Equation 8 is the extended theoretical formula for the gradient potential biased FIDA. Theoretical photon statistics $P(k)$ can be calculated by the inverse Fourier transformation of $G(\xi)$.

2.4. Extended PCH. PCH calculates the photon count spectra $P(k)$ in a quite different manner.[8] First, the photon count spectra $p^{(1)}(k)$ of a single particle in a reference volume V_0 is calculated. Then, the spectra of n particles $p^{(n)}(k)$ are calculated by the convolution of $p^{(1)}(k)$. Finally, $P(k)$ is calculated as the weighted summation of $p^{(n)}(k)$ according to the number distribution of the sample molecules.

The spectra $p^{(1)}(k)$ is determined by the number distribution and the shot noise:[8]

$$p^{(1)}(k) = \int \mathrm{Poi}(k, \epsilon W(\vec{r}))p(\vec{r}) = \frac{1}{V_0}\int \mathrm{Poi}(k, \epsilon W(\vec{r}))\, d\vec{r} \qquad k > 0 \tag{9}$$

where $p(\vec{r}) = 1/V_0$ is the probability of finding the particle at $\vec{r}$. The value of $p^{(1)}(0)$ is determined by

$$1 - \sum_{k=1}^{\infty} p^{(1)}(k)$$

When there are no particles in V_0, no photons will be detected, so $p^{(0)}(k) = \delta_{k0}$. The term $p^{(n)}(k)$ is the convolution of n $p^{(1)}$, and $P(k)$ is the weighted summation of $p^{(n)}(k)$ according to the particle number distribution:[8]

$$p^{(n)}(k) = p^{(1)} \otimes \cdots \otimes p^{(1)}(k) \quad n > 1$$

where $p^{(1)} \otimes \cdots \otimes p^{(1)}(k)$ is expressed n times

$$P(k) = \sum_{n=0}^{\infty} \mathrm{Poi}(n, C_0 V_0) p^{(n)}(k) \tag{10}$$

In the presence of a laser gradient potential, $p(\vec{r})$ is proportional to the equilibrium concentration $C(\vec{r})$. We chose $p(\vec{r})$ as

$$p(\vec{r}) = \frac{e^{\theta W(\vec{r})}}{V_0}. \tag{11}$$

There is no need to consider the unitary condition of $p(\vec{r})$, since V_0 will be canceled out in later calculations. Then, the extended PCH formula can be calculated by

$$p^{(1)}(k) = \frac{1}{V_0}\int \mathrm{Poi}(k, \epsilon W(\vec{r}))\mathrm{e}^{\theta W(\vec{r})}\,\mathrm{d}\vec{r} \quad k > 0 \qquad (12)$$

3. Methods

3.1. Simulations. As has been discussed in a previous publication,[24] experiments must be carefully designed for quantitative analysis of biased FFS measurements. There are two possible experimental implementations: the double-beam scheme[21,14] and the single-beam scheme.[15,22] Either scheme has its difficulties. The former requires precise beam alignment. The latter may suffer from excitation saturation. In this work, the theory is tested using data generated by Monte Carlo simulations.[27] The simulation program has been successfully used to study the effects of a laser gradient field on FCS experiments[23,24] and some other applications.[28,29]

Simulations of the gradient field is based on the following analysis:[23] if the step time of the simulation is small enough so that the gradient force $\vec{F}$ during each step is approximately constant, the diffusion dynamics is determined by

$$P(\vec{r}, \vec{r}_0, \tau) = (4\pi D\tau)^{-3/2}\exp\left[-\frac{\left(\vec{r} - \vec{r}_0 - \frac{D\vec{F}}{k_\mathrm{B}T}\tau\right)^2}{4D\tau}\right] \qquad (13)$$

where D is the diffusion coefficient of the sample molecules. $P(\vec{r}, \vec{r}_0, \tau)$ represents the probability that a particle starting from $\vec{r}_0$ diffuses to $\vec{r}$ after a time period τ.

In the simulations, a three-dimensional Gaussian excitation distribution is assumed,[8,30] whose radial and axial beam waists are set to be w_0 and z_0, respectively. Simulations are carried out in a $10 \times 10 \times 30$ w_0^3 box with the total particle number of 100 and $z_0 = 3w_0$, which gives $N = 0.556833$ without the gradient potential. As θ increases, the number of particles and the local concentration within the focal volume increases. Since the total particle number stays constant, the particle number and the concentration out of the focal volume, i.e., the macroscopic concentration C_0, decreases. In the calculations presented in this work, the theoretical values of N are corrected according to different values of θ. If not specifically stated, brightness of the sample is chosen as $\epsilon = 3.2$.

The sampling time (simulation step time) T_s is chosen as $0.001\tau_\mathrm{D}$. A total of $2^{27}(\approx 1.3 \times 10^8)$ steps are iterated in the simulations. Photon counting distributions of the simulated spectra are also calculated by the same program.

3.2. Data Analysis. The simulated photon counting spectra are fitted to the extended formulas and their conventional counterparts for comparison. Matlab software is used in the data analysis. The theoretical distribution $P(k)$ is calculated numerically by Matlab MEX C programming. The functions "nlinfit" and "nlparci" in the statistics toolbox are used to fit data. We use a reduced χ^2 to characterize the goodness of the fittings. The variance is chosen to be the same as that for PCH:[8]

$$\sigma_k^2 = \frac{P(k)(1 - P(k))}{M} \qquad (14)$$

where M is the number of photon counts used to build the histogram.

PCH and FIDA theoretical histograms are currently calculated by numerical integrations. In a work to be published, however, we have found that both PCH and FIDA formulas for a three-dimensional Gaussian (3DG) PSF can be expanded into a power series, which significantly improves the speed and the precision of the calculations. Similar expansions can be applied to the extended theories:

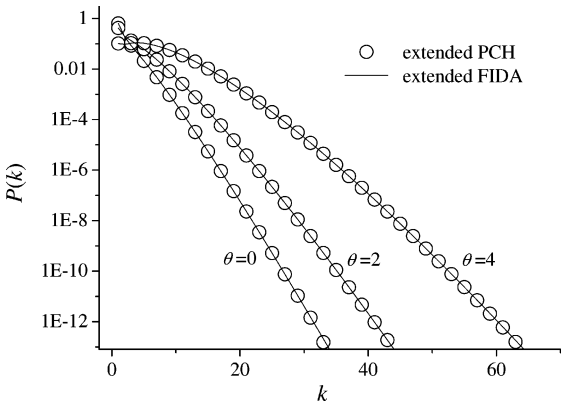

Figure 1. Comparison of extended FIDA and PCH theoretical histograms with $\epsilon = 3.2$, $N = 0.5568$ (uncorrected), and $\theta = 0$, 2, and 4, respectively.

$$\ln G(\xi) = \frac{N}{\sqrt{8}}\sum_{n=1}^{\infty}\sum_{m=0}^{\infty}\frac{(\xi - 1)^n}{m!n!(m+n)^{3/2}}\epsilon^n\theta^m \qquad (15)$$

and

$$p^{(1)}(k) = \frac{1}{\sqrt{8}}\frac{\epsilon^k}{k!}\sum_{n=0}^{\infty}\frac{(\theta - \epsilon)^n}{n!(n+k)^{3/2}} \qquad (16)$$

In the derivations, we chose V_0 as the focal volume. Coefficients of ϵ and θ can be calculated in advance to save the fitting time.

4. Results

4.1. Comparison of the Two Theories. Photon count spectra for different values of θ are calculated by the extended PCH and FIDA.

As Figure 1 shows, the histograms calculated by the two theories coincide with each other, which indicates that the two independently developed theories are numerically equivalent. It is also found that fittings to the two theories give almost the same results. So, we will only show the results of FIDA analysis in the later part of this paper.

4.2. Single-Component Tests. We first use our model to analyze photon counting spectra with only one component. In the simulations, we set $\epsilon = 3.2$ and $\theta = 0$, 1, 2, 3, and 4, respectively, representing five different molecular species or five different laser intensities for a single type of molecule. We also fitted the spectra to the conventional FIDA and PCH models for comparison. Spectra and fitted curves are shown in Figure 2. Retrieved parameters are shown in Table 1.

Figure 2 shows that the gradient field can introduce evident changes in the photon counting statistics when its potential is comparable to the thermal energy. Distributions of the photon counting statistics become broader with higher θ. Figure 2 and Table 1 show that the extended model can fit such biased spectra and retrieve the unbiased parameters. Though increase in the reduced χ^2 with θ indicates the existence of systematic errors in the fittings, the fitted parameters agree well with those set in the simulations (the maximum relative error is less than 4%).

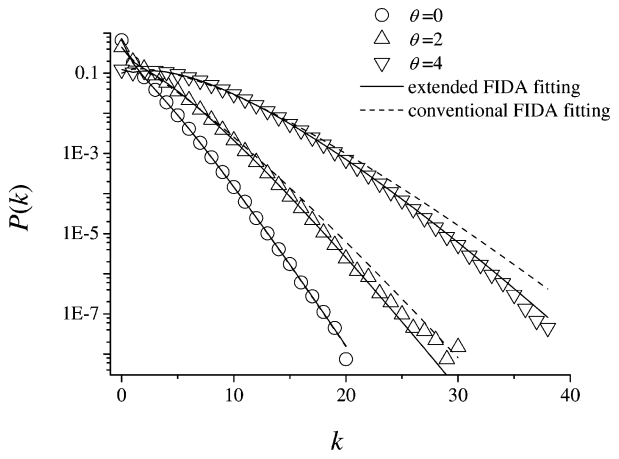

Figure 2. Fittings of simulated single-component photon counting spectra to the extended and conventional FIDA formulas. The spectra are simulated with the same ϵ (3.2) and N (0.5568, uncorrected) values but different values of θ.

Fittings to the conventional FIDA result in large errors in the retrieved parameters and much larger χ^2 values when $\theta \neq 0$.

4.3. Double-Component Tests. In heterogeneous systems, conventional FFS distinguish different particles by their differences in D (or, equivalently, the diffusion time τ_D) and ϵ. In the presence of a gradient field, FFS spectra from components of the same D and ϵ but different θ can be quite different. In this case, θ can be used as another parameter to distinguish different particles in a multiple-component solution.

To test this idea, we simulate spectra for a double-component system of the same D and ϵ but different θ and, then, fit the spectra to the double-component variation of the extended FIDA formula. To achieve robust fittings, ϵ and θ of the two components (ϵ_1, θ_1, ϵ_2, and θ_2) have to be determined in advance, e.g., by single-component pre-experiments as described in section 4.2. N_1 and N_2 are to be determined by the fittings.

First, we take a double-component system of equal concentration but different polarizabilities. We set $N_1 = N_2 = 0.278\,416$ (50 particles for each component in the simulation region), $\epsilon_1 = \epsilon_2 = 3.2$, and $\theta_1 = 1$ and, then, vary θ_2 in different simulations. The simulated spectra and the fitted curves with $\theta_2 = 2$, 3, and 4 are shown in Figure 3.

We can see from Figure 3 that the double-component spectra can be fitted without evident discrepancy. The retrieved concentrations are plotted against the ratio of the polarizabilities of the two components in Figure 4, which shows that the errors first decrease as the ratio of the polarizabilities increases and, then, level off.

Then, we tested the theory using mixtures with two components of different concentrations. The concentration ratio N_1:N_2 is set to 1:9, 3:7, 5:5, 7:3, and 9:1, respectively. The total concentration of the two components remains the same ($N_1 + N_2 = 0.556833$). In the simulations, $\theta_1 = 1$ and $\theta_2 = 3$ are set. The errors in the retrieved concentrations are plotted against the concentration ratio in Figure 5, which shows that the relative error of a component decreases when it takes a larger portion in the mixture.

4.4. Simulation Error. Though the single-component fittings gave satisfactory results, the sharp increase in the reduced χ^2 shows that there is a systematic discrepancy between the simulation and the theoretical calculation. The double-component fittings show that the retrieved concentration of the component with higher polarizability is higher than the true value. This further indicates the existence of a systematic error.

To test the discrepancy, simulations are carried on for a high brightness ($\epsilon = 9.6$) sample in a strong gradient potential ($\theta = 6.0$).

We can see from the results (Figure 6) evident deviations between the simulated spectra and the theoretical predication. The discrepancy is attributed to the simulation algorithm. In the current algorithm, the total particle number is kept constant during the simulations. In real equilibrium systems, however, the particle number in any spatial volume follows the Poisson distribution.

Figure 7 shows the particle number distribution in the focal volume and its deviation from the predicted Poisson distributions. In the simulations, we assumed that the focal volume is a spheroid with a volume of $\pi^{3/2}w_0^2z_0$ as defined in the FFS literature. After each step of the simulation, the number of the particles in the volume is recorded. Then, all the recorded particle numbers are analyzed and plotted on completion of the simulation.

The current simulation program treats the total particle number in the simulation volume as a constant instead of a distribution, so the particle number distribution in the focal volume (Figure 7) and the photon counting statistics (Figure 6) in the simulations are narrower than the theoretical distributions. As θ increase, larger portion of the particles will be attracted into the focal volume (from less than 0.6% to more than 8.2% in Figure 7), which causes a larger discrepancy in the results.

One may improve the accuracy of the simulations with larger simulation volumes at the same concentration. However, larger simulation volumes means more particles for the simulation and longer simulation time. One has to consider the tradeoff between the precision and the time consumption in the simulations.

5. Discussions

5.1. Equivalence of Extended FIDA and PCH Analysis. The results in section 4 indicate that the extended FIDA and PCH are numerically equivalent. We can prove that the two extended theories are also theoretically equivalent for any choices of PSFs.

We can calculate the generating function of $P(k)$ in PCH as follows:

$$G^{(1)}(\xi) = \sum_{k=0}^{\infty} p^{(1)}(k)\xi^k = 1 + \sum_{k=1}^{\infty} p^{(1)}(k)(\xi^k - 1)$$

$$G^{(n)}(\xi) = [G^{(1)}(\xi)]^n$$

$$G(\xi) = \sum_{n=0}^{\infty} \mathrm{Poi}(n, N) G^{(n)}(\xi) = \exp[-N + NG^{(1)}(\xi)]$$

$$\ln G(\xi) = C_0 \int \sum_{k=1}^{\infty} \frac{(\epsilon W)^k \mathrm{e}^{-\epsilon W}}{k!} \mathrm{e}^{\theta W}(\xi^k - 1)\, \mathrm{d}\vec{r} = C_0 \int (\mathrm{e}^{\epsilon W(\xi-1)} - 1)\mathrm{e}^{\theta W}\, \mathrm{d}\vec{r} \quad (17)$$

This formula is exactly the same as that of FIDA (eq 8).

5.2. Practical Implementations. In the current theoretical framework, we take into account only the simplest case, where the excitation laser intensity, the gradient potential, and the PSFs all follow 3DG distributions. In real experiments, however, the shape of a PSF is often different from that of the gradient potential $U(\vec{r})$. $U(\vec{r})$ has to be modified in the specific experimental systems. A PSF may also take different forms in different detection schemes. Though the 3DG distribution is widely adopted in one-photon excitation FFS, many have shown that

TABLE 1: Fitted Parameters from Simulated Single-Component Photon Counting Spectra (Figure 2)[a]

set		extended FIDA				conventional FIDA		
θ	N	N	ϵ	θ	χ^2	N	ϵ	χ^2
0	0.5568	0.563 ± 0.002	3.20 ± 0.02	−0.05 ± 0.03	0.8	0.559	3.17	1.1
1	0.5555	0.557 ± 0.002	3.23 ± 0.01	0.96 ± 0.02	1.0	0.652	3.98	3 847.5
2	0.5535	0.559 ± 0.005	3.13 ± 0.02	2.04 ± 0.03	3.0	0.868	4.78	20 285.5
3	0.5502	0.546 ± 0.011	3.15 ± 0.03	3.05 ± 0.05	8.2	1.246	5.63	50 588.3
4	0.5443	0.544 ± 0.034	3.12 ± 0.05	4.05 ± 0.12	26.8	2.139	6.03	53 461.1

[a] The spectra are simulated with the same ϵ (3.2) but different values of θ. N decreases slightly with θ because of the limited total number of particles in the simulations.

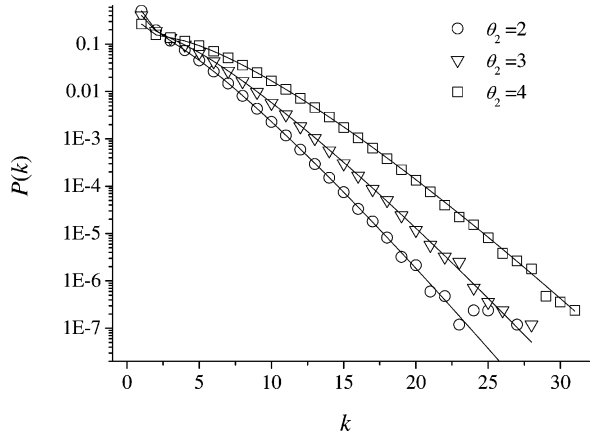

Figure 3. Fittings of the simulated double-component photon counting spectra. The two components are of equal concentration (50 particles each in the simulation region) and brightness (3.2) but different polarizabilities.

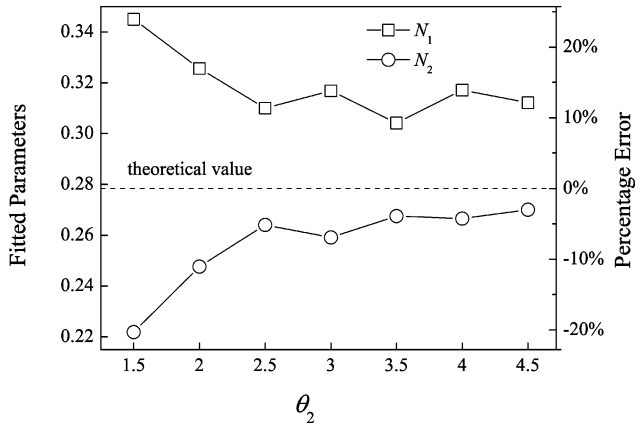

Figure 4. Relative errors of the fitted concentrations of the double-component solution shown in Figure 3.

using 3DG in PCH may fail to fit the experimental data.[30−32] Actually, the presented theories are flexible enough to handle the general cases. In both FIDA and PCH analysis, a PSF can be treated in three approaches: The first approach is to calculate or measure the exact form of the PSF $W(\vec{r})$ and, then, to calculate $P(k)$ using eq 8 and/or eq 12. This approach can be very precise but is very computation intensive. The second approach is to model the PSF by a general expression $dV(x)/dx$. Though it is mostly used in FIDA, this approach also applies to PCH. We rewrite eqs 8 and 12 as

$$\ln G(\xi; N, \epsilon) = \int_0^\infty C_0\{\exp[(\xi - 1)\epsilon e^{-x}] - 1\} e^{\theta_e e^{-x}} \frac{dV(x)}{dx} dx \quad (18)$$

and

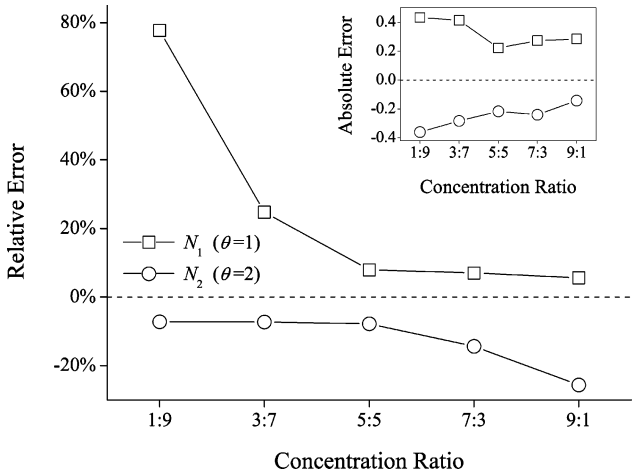

Figure 5. Relative errors of the fitted concentrations of two-component solutions with different concentration ratios. In the simulations, $\theta_1 = 1$, $\theta_2 = 3$, and $\epsilon_1 = \epsilon_2 = 3.2$ are set. Absolute errors are plotted in the inset.

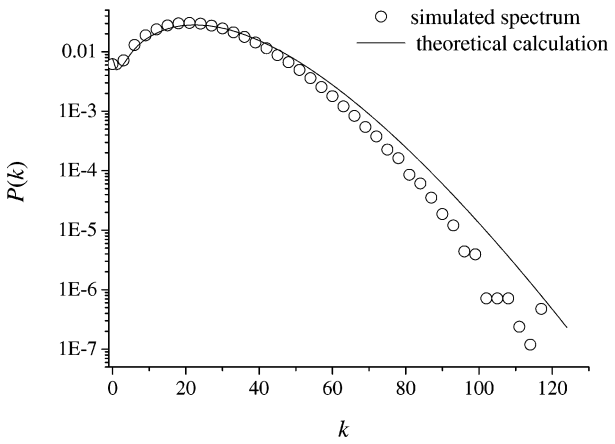

Figure 6. Discrepancy between the simulation and the theoretical histogram with large values of ϵ (9.6) and θ (6.0).

$$p^{(1)}(k) = \frac{1}{V_0}\int_0^\infty \mathrm{Poi}(k, \epsilon e^{-x}) e^{\theta_e e^{-x}} \frac{dV(x)}{dx} dx \quad (19)$$

In some cases, $dV(x)/dx$ can be derived analytically. For example, $dV(x)/dx = V\sqrt{x}/2\pi$ for the 3DG PSF. Generally, $dV(x)/dx$ can be chosen as $\sum_k a_k x^k$. Values of a_k are to be determined by calibration experiments on known systems. This approach is very flexible but lacks physical insight. The last approach builds the PSF on the basis of known distributions, e.g., the 3DG distribution. The Zare group introduced the parameter F_j, which is the relative error in the jth power of $W(\vec{r})$, to correct the 3DG PSF in one-photon PCH experiments.[32,30] We can see that both eqs 8 and 12 can be expressed as power series of $W(\vec{r})$, so this approach can also be exploited in the extended FIDA and PCH theories.

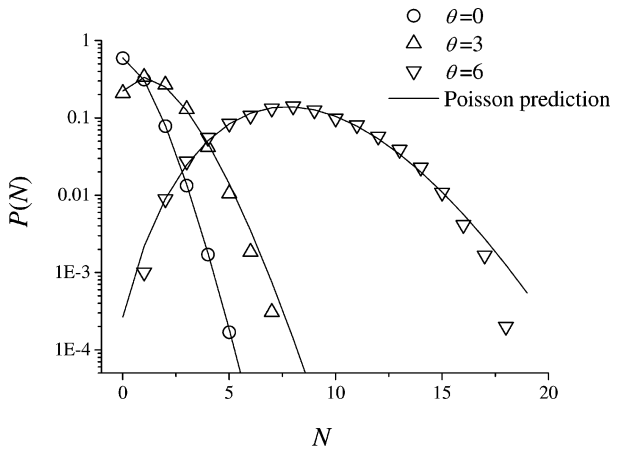

Figure 7. Particle number distributions in the focal volume. Simulated distributions are narrower than the theoretical prediction due to the fixed total particle number. The deviation becomes evident as θ increases. The brightness of the sample is 3.2.

The presented theories only deal with the laser gradient force, while they neglect the scattering force and particle−particle interactions such as the optical binding force.[33,34] In fact, the theories generally apply to situations where the total force can be described by a potential well so that the concentration can reach equilibrium. In typical single beam traps where the gradient force dominates the other forces, this requirement is satisfied. However, the presence of other forces may distort the shape of the potential well and perturb the concentration distribution.

The extended theories of PCH and FIDA can also be applied in parallel to FCS analysis. In previous studies, we have treated the effect of a gradient field in the FCS measurements and retrieved unbiased N and τ_D, the diffusion time, as well as θ.[24] Many approximations have to be used in the treatment, which make the fitting procedure complicated and, sometimes, unstable. The extended FIDA and PCH approaches do not rely on approximations and, therefore, are much more robust. Since FCS and photon counting statistical methods are complementary, they may be applied in parallel. Data from a FFS experiment in the gradient field may be analyzed at first with FIDA or PCH to retrieve the particle number N and the trapping coefficient θ. These values are then used in FCS fittings to retrieve τ_D. The two complimentary approaches may also be used together in multiple-component systems.

5.3. Possible Applications. In the presence of a laser gradient field, the diffusion dynamics of the sample molecules is disturbed and the detected photon count statistics are biased. Both the width and the mean value of the photon count distribution increase, as is shown in Figure 2. The effects of a laser gradient field can be described by a gradient coefficient, θ.

Although few data have been reported for the polarizabilities of biomolecules, we may have a coarse estimate. Osborne et al.[15] estimated that θ for the Rhodamine 6G molecule is around 3 times the laser power (in mW) incident at the sample (514.5 nm excitation and an objective with NA = 1.3 were used). The estimation of Chirico et al.[22] is of the same order. According to their results, a 10 mW focused laser beam can result in a θ value around the magnitude of 1, whose effects are evidently perceptible as shown in Figure 2. Moreover, dielectric beads are often used as handles when biomolecules such as DNA or proteins are manipulated by optical traps. The polarizability of a bead is controlled by its size and can be very large.

Using the modified formulas, one can retrieve the unbiased N and ϵ as well as θ by fitting the biased photon counting spectra. This provides us with the ability to evaluate the interaction between the optical field and the particles as well as to measure the actual local concentration and the particle brightness from biased detections.

We also showed the possibility to differentiate particle species by θ (hence, the polarizability α). It is known that FCS distinguishes contributions from different components in a mixture by their difference in diffusion time τ_D (hence, the diffusion coefficient D), while PCH and FIDA differentiate by brightness ϵ. As shown in Figure 2, in the presence of a laser gradient field, θ has evident effects on the photon counting statistics, so it may help to retrieve the concentrations of each component in a mixture. Though results in Figures 4 and 5 are still primitive and further studies are still needed before the implementation, they offer information on the effects of the polarizability and concentration ratio when dealing with multiple-component systems. For trapping schemes using beads, whose θ values are related to their sizes, biomolecules attached to different beads can be practically resolved by a gradient field. The technique of trapping large molecules without the assistance of bead handles[14,35] may open new opportunities for this method. Since the polarizability is closely related to the electronic cloud distribution or the electronic structure of the molecule, this method may also be used to monitor the dynamical changes of the conformation of the trapped biomolecules.

Acknowledgment. This work was supported by the National Natural Science Foundation of China under Grants 19928408, 60138010, and 10274039.

References and Notes

(1) Van Orden, A.; Fogarty, K.; Jung, J. Fluorescence fluctuation spectroscopy: A coming of age story. *Appl. Spectrosc.* **2004**, *58* (5), 122A−137A.

(2) Magde, D.; Elson, E.; Webb, W. W. Thermodynamic fluctuations in a reacting system: Measurement by fluorescence correlation spectroscopy. *Phys. Rev. Lett.* **1972**, *29* (11), 705−708.

(3) Berland, K. M.; So, P. T. C.; Gratton, E. Two-photon fluorescence correlation spectroscopy − Method and application to the intracellular environment. *Biophys. J.* **1995**, *68* (2), 694−701.

(4) Schwille, P.; Korlach, J.; Webb, W. W. Fluorescence correlation spectroscopy with single-molecule sensitivity on cell and model membranes. *Cytometry* **1999**, *36* (3), 176−182.

(5) Schwille, P. Fluorescence correlation spectroscopy and its potential for intracellular applications. *Cell. Biochem. Biophys.* **2001**, *34* (3), 383−408.

(6) Hess, S. T.; Huang, S. H.; Heikal, A. A.; Webb, W. W. Biological and chemical applications of fluorescence correlation spectroscopy: A review. *Biochemistry* **2002**, *41* (3), 697−705.

(7) Chen, Y.; Wei, L. N.; Muller, J. D. Probing protein oligomerization in living cells with fluorescence fluctuation spectroscopy. *Proc. Natl. Acad. Sci. USA* **2003**, *100* (26), 15492−15497.

(8) Chen, Y.; Muller, J. D.; So, P. T. C.; Gratton, E. The photon counting histogram in fluorescence fluctuation spectroscopy. *Biophys. J.* **1999**, *77* (1), 553−567.

(9) Kask, P.; Palo, K.; Ullmann, D.; Gall, K. Fluorescence-intensity distribution analysis and its application in biomolecular detection technology. *Proc. Natl. Acad. Sci. USA* **1999**, *96* (24), 13756−13761.

(10) Ashkin, A.; Dziedzic, J. M.; Bjorkholm, J. E.; Chu, S. Observation of a single-beam gradient force optical trap for dielectric particles. *Opt. Lett.* **1986**, *11* (5), 288−290.

(11) Ashkin, A. Optical trapping and manipulation of neutral particles using lasers. *Proc. Natl. Acad. Sci. USA* **1997**, *94* (10), 4853−4860.

(12) Ashkin, A. Forces of a single-beam gradient laser trap on a dielectric sphere in the ray optics regime. *Methods Cell Biol.* **1998**, *55*, 1−27.

(13) Neuman, K. C.; Block, S. M. Optical trapping. *Rev. Sci. Instrum.* **2004**, *75* (9), 2787−2809.

(14) Chiu, D. T.; Zare, R. N. Biased diffusion, optical trapping, and manipulation of single molecules in solution. *J. Am. Chem. Soc.* **1996**, *118* (27), 6512−6513.

(15) Osborne, M. A.; Balasubramanian, S.; Furey, W. S.; Klenerman, D. Optically biased diffusion of single molecules studied by confocal fluorescence microscopy. *J. Phys. Chem. B* **1998**, *102* (17), 3160−3167.

(16) Kuyper, C. L.; Chiu, D. T. Optical trapping: A versatile technique for biomanipulation. *Appl. Spectrosc.* **2002**, *56* (11), 300A−312A.

(17) Grier, D. G. A revolution in optical manipulation. *Nature* **2003**, *424* (6950), 810−816.

(18) Cherney, D. P.; Bridges, T. E.; Harris, J. M. Optical trapping of unilamellar phospholipid vesicles: Investigation of the effect of optical forces on the lipid membrane shape by confocal-raman microscopy. *Anal. Chem.* **2004**, *76* (17), 4920−4928.

(19) Svoboda, K.; Mitra, P. P.; Block, S. M. Fluctuation analysis of motor protein movement and single enzyme-kinetics. *Proc. Natl. Acad. Sci. USA* **1994**, *91* (25), 11782−11786.

(20) Hosokawa, C.; Yoshikawa, H.; Masuhara, H. Cluster formation of nanoparticles in an optical trap studied by fluorescence correlation spectroscopy. *Phys. Rev. E* **2005**, *72* (2), Article No. 021408.

(21) Ding, Y.; Meng, F. B.; Chen, B.; Ma, H.; Lei, J.; Chen, D. Y. An experimental study on the fluorescence correlation spectroscopy in laser gradient field. *Acta Phys. Sin.* **2001**, *50* (11), 2269−2274.

(22) Chirico, G.; Fumagalli, C.; Baldini, G. Trapped brownian motion in single- and two-photon excitation fluorescence correlation experiments. *J. Phys. Chem. B* **2002**, *106* (10), 2508−2519.

(23) Meng, F. B.; Chen, B.; Liu, G.; Ma, H. Diffusion in laser gradient field studied by fluorescence correlation spectroscopy. *Chin. Phys. Lett.* **2004**, *21* (4), 760−763.

(24) Meng, F. B.; Ma, H. Fluorescence correlation spectroscopy analysis of diffusion in laser gradient field: A numerical approach. *J. Phys. Chem. B* **2005**, *109* (12), 5580−5585.

(25) Chirico, G. Effect of a trapping force on a photon-counting histogram. *Appl. Opt.* **2002**, *41*(4), 593−600.

(26) Risken, H. *The Fokker−Planck equation: Methods of solution and applications*, 2nd ed.; Springer-Verlag: New York, 1989.

(27) Meng, F. B.; Chen, B.; Liu, G.; Ding, J. Y.; Ma, H. Fluorescence fluctuation spectroscopy and its artifacts: simulations and tests. *Sci. China G* **2005**, *48* (3), 336−344.

(28) Ding, J. Y.; Chen, B.; Meng, F. B.; Ma, H. Fluorescence correlation spectroscopy with saturated excitation. *Acta Phys. Sin.* **2004**, *53* (8), 2503−2508.

(29) Liu, G.; Chen, B.; Meng, F. B.; Ma, H.; Chen, D. Y. Fluorescence fluctuation spectroscopy with strong background fluorescence − an monte carlo approach. *Spectrosc. Spect. Anal.* **2004**, *24* (11), 1379−1383.

(30) Huang, B.; Perroud, T. D.; Zare, R. N. Photon counting histogram: One-photon excitation. *Chemphyschem* **2004**, *5* (10), 1523−1531.

(31) Van Rompaey, E.; Chen, Y.; Muller, J. D.; Gratton, E.; Van Craenenbroeck, E.; Engelborghs, Y.; De Smedt, S.; Demeester, J. Fluorescence fluctuation analysis for the study of interactions between oligonucleotides and polycationic polymers. *Biol. Chem.* **2001**, *382* (3), 379−386.

(32) Perroud, T. D.; Huang, B.; Wallace, M. I.; Zare, R. N. Photon counting histogram for one-photon excitation. *Chemphyschem* **2003**, *4* (10), 1121−1123.

(33) Burns, M. L.; Fournier, J. M.; Colovchenko, J. A. Optical binding. *Phys. Rev. Lett.* **1989**, *63* (12), 1233−1236.

(34) Mohanty, S. K.; Andrews, J. T.; Gupta, P. K. Optical binding between dielectric particles. *Opt. Express* **2004**, *12* (12), 2749−2756.

(35) Katsura, S.; Hirano, K.; Matsuzawa, Y.; Yoshikawa, K.; Mizuno, A. Direct laser trapping of single dna molecules in the globular state. *Nucleic Acids Res.* **1998**, *26* (21), 4943−4945.